EDGE ARTICLE

Solution structural characterization of an array of nanoscale aqueous inorganic $Ga_{13-x}In_x$ (0 ≤ x ≤ 6) clusters by ^{1}H-NMR and QM computations†

Anna F. Oliveri,[a] Lindsay A. Wills,[b] Caitlyn R. Hazlett,[a] Matthew E. Carnes,[a] I-Ya Chang,[b] Paul Ha-Yeon Cheong*[b] and Darren W. Johnson*[a]

NMR spectroscopy is the go-to technique for determining the solution structures of organic, organometallic, and even macromolecular species. However, structure determination of nanoscale aqueous inorganic clusters by NMR spectroscopy remains an unexplored territory. The few hydroxo-bridged inorganic species well characterized by ^{1}H Nuclear Magnetic Resonance spectroscopy (^{1}H-NMR) do not provide enough information for signal assignment and prediction of new samples. ^{1}H-NMR and quantum mechanical (QM) computations were used to characterize the NMR spectra of the entire array of inorganic flat-$Ga_{13-x}In_x$ (0 ≤ x ≤ 6) nanoscale clusters in solution. A brief review of the known signals for μ_2-OH and μ_3-OH bridges gives expected ranges for certain types of protons, but does not give enough information for exact peak assignment. Integration values and NOESY data were used to assign the peaks of several cluster species with simple ^{1}H-NMR spectra. Computations agree with these hydroxide signal assignments and allow for assignment of the complex spectra arising from the remaining cluster species. This work shows that ^{1}H-NMR spectroscopy provides a variety of information about the solution behavior of inorganic species previously thought to be inaccessible by NMR due to fast ligand and/or proton exchange in wet solvents.

Introduction

Proton Nuclear Magnetic Resonance spectroscopy (^{1}H-NMR) is an important tool heavily utilized by chemists and biochemists since its discovery in 1945.[1] Unfortunately, it is often not a viable technique for characterizing purely inorganic clusters due to the fast exchange of protons and/or ligands in aqueous coordination clusters dissolved in wet/polar solvents. The reliable trends and generalizations in ^{1}H-NMR shifts tabulated for numerous carbon-containing molecules do not translate to this purely inorganic world. The focus of this manuscript is to correlate the ^{1}H-NMR spectral shifts of nanoscale aqueous clusters dissolved in wet solvents to their hydroxo ligands to substantiate cluster characterization and speciation in solution. The ^{1}H-NMR spectrum of $[Ga_{13}(\mu_3\text{-OH})_6(\mu_2\text{-OH})_{18}(H_2O)_{24}]$-$(NO_3)_{15}$ (**Ga13**) in wet d_6-DMSO is known.[2] Due to the spectral complexity, no peaks were assigned to specific hydroxo and aquo protons in the structure at that time. Further

analysis coupled with computations of the complete series of $[Ga_{13-x}In_x(\mu_3\text{-OH})_6(\mu_2\text{-OH})_{18}(H_2O)_{24}]$-$(NO_3)_{15}$ clusters (1 ≤ x ≤ 6: **Ga12In1, Ga11In2, Ga10In3, Ga9In4, Ga8In5, Ga7In6**) provides trends and clarity, allowing partial ^{1}H signal assignment and complete assignment of all hydroxo bridges in the "mother clusters" (*i.e.*, clusters entirely capped with water molecules that potentially undergo exchange with coordinating solvents, Fig. 1).

^{1}H-NMR spectroscopy is the first characterization technique used in modern organic, organometallic, and coordination
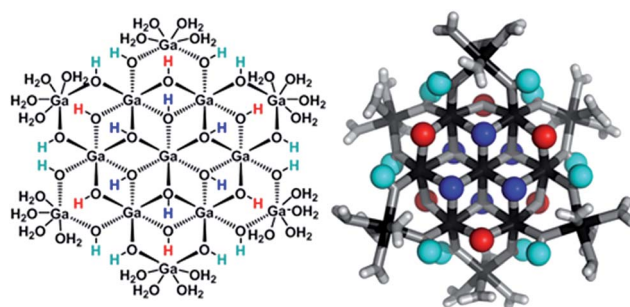
[a] Department of Chemistry & Biochemistry and Materials Science Institute, University of Oregon, Eugene, Oregon 97403-1253, USA. E-mail: dwj@uoregon.edu

[b] Department of Chemistry, Oregon State University, 153 Gilbert Hall, Corvallis, Oregon 97331-4003, USA. E-mail: paulc@science.oregonstate.edu; Web: http://sustainablematerialschemistry.org

Fig. 1 Structure of $Ga_{13-x}In_x$ (0 ≤ x ≤ 6, pictured x = 0) mother clusters. Left: full bonding scheme for clusters including atom identity. Right: top view of 3 dimensional structure depicting 3 types of hydroxide bridges. The μ_3-OH are blue, internal μ_2-OH are red, and external μ_2-OH are cyan.

chemistry, yet such data are only sporadically reported for aqueous inorganic clusters. We have found that under the right conditions such clusters often exhibit rich ^{1}H-NMR spectra that enable characterization by 2D NMR techniques as well.[2] A bottleneck in determining solution structure by NMR spectroscopy has been the lack of tabulated data for such clusters and predictive methods for peak assignment. For instance, there is no known way for predicting where M − H$_2$O or M–(μ_2-OH)–M ^{1}H-NMR signals should resonate like there is for organic compounds. In this manuscript we provide a literature survey of ^{1}H-NMR spectroscopic resonances reported for known hydroxo- and aquo-coordinated metal complexes. To the best of our knowledge, such data have not been aggregated in one location. We then use this information and complementary quantum mechanical (QM) computations to provide the complete solution structure and peak assignment for a series of clusters.

The Ga$_{13-x}$In$_x$ clusters in this work are completely inorganic. Clusters of this type are often more difficult to isolate and challenging to characterize[13] than organic ligand-supported versions, because the ligands lower the cluster charge and can increase stability.[14] However, the lack of organic ligands makes these species attractive candidates as precursors (inks) for metal oxide films, as the lack of organic additives that must be "burned" off during film formation/condensation leads to fewer defects and increases density of thin films. These clusters also serve as excellent inks/precursors due to their high solubility in aqueous and alcoholic solutions, which eliminates toxic solvents often used in thin film production. Minimizing the organic ligands for such applications has produced superior precursors,[13] but the lack of spectroscopic handles has limited the complete understanding of the solution behavior of these species.

Previously, single crystal X-ray diffraction (XRD) and elemental analysis were the techniques used to differentiate the seven known flat-Ga$_{13-x}$In$_x$ clusters.[15] These techniques suggest that multiple cluster species might co-crystallize during isolation (for example, Ga$_{10.2}$In$_{2.8}$ has been isolated, which could be an 80/20 mixture of Ga$_{10}$In$_3$ and Ga$_{11}$In$_2$ or some other such combination). Ga$_{13}$ has been recently characterized in solution using NMR, Small Angle X-ray Scattering (SAXS), and Raman.[2,16] Although single crystal XRD can provide excellent solid-state data, it cannot answer pressing current questions. Does Ga$_{10}$In$_3$ even exist or are all of the mixed clusters simply various ratios of

Ga$_{13}$ and Ga$_7$In$_6$? Do all of the possible isomers in the Ga$_9$In$_4$–Ga$_{11}$In$_2$ clusters (Fig. 1) co-crystallize or are certain ones thermodynamically favored? Is there a way to determine the ratio of isomers present in a sample? Using ^{1}H-NMR, we have established a quick technique for characterizing samples that could address these questions and will accelerate the synthesis and identification of cluster species in solution.

^{1}H-NMR spectra of hydroxo/aquo bridged coordination compounds

Only a limited number of reports of completely inorganic, hydroxo bridged species have been studied *via* ^{1}H-NMR spectroscopy. However, the moderate chemical shift library of hydroxo protons identified in ligand-supported metal complexes and coordinated water allows for some comparison. The typical chemical shifts of coordinated water ligands are generally downfield (Table 1). Typically hexaaquo species have proton signals in the range of 8.3 to 11.3 ppm, while water ligands on metal oligomers tend to appear slightly upfield between 6.3 and 10 ppm.

Little is known about the potential trends for these hydroxide bridges in inorganic species, although it appears that the metal atom and its coordination number are main contributors to the chemical shift of these hydroxo protons. The collected chemical shifts have been tabulated and discussed for the readers benefit (Tables 2–5). For diamagnetic complexes, μ_2-OH protons fall between −4.5 and 7 ppm; while μ_3-OH proton signals occur from −1.05 to 6.79 ppm (Fig. 2). The observation of these ^{1}H-NMR signals at lower chemical shifts than that of the hexaaquo species and the free hydroxide ions is caused by the increased electron density around the proton in the bridge.[5] These are fairly large regions that are not distinguishable from one another, but can be differentiated from water ligands. By looking more closely at specific metals, coordination environments, and groups on the periodic table, refined assignments of chemical shift regions and apparent trends emerge.

Octahedral M(III) ions (M = Al, Ga, Ir, Rh, and W), the most relevant for this work, tend to produce signals for μ_2-OH protons that range from 1.5–5.0 ppm, although this does not hold true for Co(III).[17–21] Geometries, chemical shift data, and available NMR conditions for these metal complexes are shown in Table 2. The majority of this data was referenced to TMS or

Table 1 ^{1}H-NMR data for water ligands bound to metal atoms

Metal	Type of complex	Chem. shift (ppm)	NMR conditions	Ref.
Al^{III}	Hexaaquo	10.2	d_6-Acetone; 400 MHz	3
Ga^{III}	Hexaaquo	8.3	d_6-Acetone; −50 °C; 500 Hz	4
Rh^{III}	Hexaaquo	9.0–9.2	d_6-Acetone; −83 °C; 400 MHz	5
Sn^{IV}	Hexaaquo	10.1–11.3	d_6-Acetone; −100 °C; 60 MHz	6
Al^{III}	Oligomer (Al$_{13}$-Keggin)	7.5	d_6-Acetone; −30 °C; 400 MHz	7
Al^{III}	Oligomer (Al$_{13}$-Keggin)	6.3	d_3-Acetonitrile; 400 MHz	7
Al^{III}	Oligomer (Al$_{13}$-Keggin)	8.0	H$_2$O/d_6-Acetone (2.5 : 1); −20.6 to −5.2 °C; 500 MHz	8
Al^{III}	Oligomers	7–10	d_6-Acetone; 400 MHz	3
Al^{III}	Oligomers	8–9.5	—	5, 7
Rh^{III}	Oligomers	8.4, 8.7	d_6-Acetone; −83 °C; 400 MHz	5

Table 2 ^{1}H-NMR data for μ_2-OH bridges linking trivalent octahedral metals in homo-metallic complexes

Metal	Molecular geometry of M^{X+}	μ_2-OH Chem. shift (ppm)	NMR conditions	Ref.
Al^{III}	Octahedral (Al$_{13}$-Keggin)	3.8, 3.9	d_6-Acetone; −30 °C; 400 MHz	7
Al^{III}	Octahedral (Al$_{13}$-Keggin)	2.8, 3.0	d_3-Acetonitrile; 400 MHz	7
Al^{III}	Octahedral (Al$_{13}$-Keggin)	3.8, 4.5	H$_2$O/d_6-Acetone (2.5 : 1); −20.6 to −5.2 °C; 500 MHz	8
Al^{III}	Octahedral (Al$_{13}$-Keggin)	3.8	H$_2$O/d_6-DMSO (2 : 1); 3.7 to 95.2 °C; 500 MHz	8
Al^{III}	Octahedral	4.8	—	5
Ga^{III}	Octahedral	2.03	d_6-DMSO; 400 MHz	9
Ga^{III}	Octahedral	4.2	d_3-Acetonitrile/D$_2$O; 250 MHz	10
Ir^{III}	Distorted octahedral	1.6	d-Chloroform; 25 °C; 270 MHz	11
Rh^{III}	Octahedral (di/trimer)	3.7, 4.3	d_6-Acetone; −83 °C; 400 MHz	5
W^{III}	Octahedral	2.05	d-Chloroform; 19 and 55 °C; 400 MHz	12

residual protic peaks described in the primary papers. Solvent and temperature do not appear to significantly affect the chemical shifts.[12]

The top section of Table 3 indicates some metal complexes with different oxidation states and/or non-octahedral geometries exhibit resonance for hydroxide bridges similar to the

Table 3 ^{1}H NMR Data for μ_2-OH bridges in homo-metallic complexes

Metal	Molecular geometry of M^{X+}	μ_2-OH Chem. shift (ppm)	NMR conditions	Ref.
Be^{II}	Tetrahedral	4.3	−55 °C; 220 MHz	22
Mg^{II}	Trigonal bipyramidal	3.99	d_8-THF; 25 °C; 300 MHz	44
Mo^{II}	Square pyramidal^b	2.44	—	45
Mo^{II}	Pentagonal bipyramidal	1.24	d_2-Dichloromethane; −78 °C; 400 MHz	46
Ru^{II}	Five coordinate^a	3.00, 2.94	d_6-Acetone; 60 & 220 MHz	47
Sn^{IV}	Trigonal bipyramidal	2.61, 3.85, 2.3	d-Chloroform; 360 & 400 MHz	36–38
W^{II}	Pentagonal bipyramidal	1.7	d_2-Dichloromethane; −78 °C; 400 MHz	46
Zn^{II}	Trigonal bipyramidal	4.16	d_3-Acetonitrile; 270 MHz	41
Zn^{II}	Octahedral	2.08	d_6-DMSO	43
Zr^{IV}	Pentagonal bipyramidal	3.8	d_8-THF; 200 MHz	48
Zr^{IV}	Octahedral^b	1.39–1.57^c	d_6-DMSO; 400 MHz	49
Cd^{II}	Trigonal bipyramidal	−2.43	d_3-Acetonitrile; 20 °C; 400 MHz	42
Co^{III}	Octahedral	−2	d_6-DMSO	17
Co^{III}	Octahedral	0.63	d_3-Acetonitrile; 250 MHz	18
Co^{III}	Octahedral	−4.18	d_6-DMSO	19
Co^{III}	Octahedral	−0.15, −2.56, −4.95	d_6-DMSO; 20 °C; 300 MHz	21
Co^{III}	Octahedral	−1.195, 1.397	d_6-DMSO; 25 °C; 600 MHz	20
Co^{III}	Octahedral	−0.702, −0.670	D$_2$O; 4 °C; 600 MHz	20
Ga^{III}	Tetrahedral	0.14	d_6-Benzene; 300 MHz	50
In^{I}	Square pyramidal	0.93	d_6-Benzene; 400 MHz	51
Os$^{0/II}$	Six/seven coordinate^a	−2.8	d_2-Dichloromethane; 400 MHz	24
Os$^{0/II}$	Octahedral	−1.98 to −0.44^c	d-Chloroform; 200 MHz	25
Pd^{II}	Square planar	−1.58, −1.66, −2.96, −3.09	—	26
Pd^{II}	Square planar	−2.84, −1.53, −1.67	d-Chloroform; 200 MHz	27
Pd^{II}	Square planar	−1.01, −1.17, −1.25	d_6-Acetone; 200 and 300 MHz	28
Pd^{II}	Square planar	−0.9, −1.0	d-Chloroform; −3 and 27 °C; 600 MHz	29
Pd^{II}	Square planar	−0.85	d-Chloroform; 200 MHz	30
Pt^{II}	Square planar	−0.14	d_2-Dichloromethane; 200 MHz	31
Pt^{II}	Square planar	−2.04, −1.22, −1.03, −0.56	d-Chloroform; 25 °C; 80 MHz	32
Pt^{II}	Square planar	1.9, −0.8, −0.46	d-Chloroform; 80 and 200 MHz	34
Pt^{II}	Square planar	2.0, −0.9, −0.45	d_2-Dichloromethane; 80 and 200 MHz	34
Pt^{II}	Square planar	2.12	d-Chloroform; 300 MHz	33
Sn^{IV}	Octahedral	7.33	d_6-DMSO; 300 MHz	39
Sn^{IV}	Octahedral	7.02	d_2-Dichloromethane; 300 MHz	39
Y^{III}	Eight coordinate^a	6.4, 5.45	d_3-Acetonitrile; 300 MHz	40
Y^{III}	Dodecahedral^b	5.4	d_3-Acetonitrile; 300 MHz	40
Y^{III}	Bicapped trig. prismatic	5.23, 5.35	d_3-Acetonitrile; 300 MHz	40
Y^{III}	Square antiprismatic^b	6.2	d_2-Dichloromethane; 300 MHz	40
Zn^{II}	Trigonal bipyramidal^b	−1.15, −0.66	d_3-Acetonitrile; 20 °C; 300 & 400 MHz	42

^{a} No indication of molecular geometry. ^{b} Distorted geometry. ^{c} Six or more proton signals in this range.

Table 4 ^{1}H NMR data for μ_2-OH bridges in hetero-metallic complexes

Metals	Molecular geometry of M^{X+}	μ_2-OH Chem. shift (ppm)	NMR conditions	Ref.
Fe^0 / \ Ru^I-(OH)-Ru^I	Octahedral	−2.16, −1.78, −1.75	d-Chloroform	52
Fe^{II} / \ Sn^{II}-(OH)-Sn^{II}	Tetrahedral	1.7	d_6-Benzene; 27 °C; 300 and 500 MHz	35
Co^{III} / \ Sn^{II}-(OH)-Sn^{II}	Tetrahedral	1.63	d_6-Benzene; 27 °C; 300 and 500 MHz	35
Ga^{III}–(OH)–Ca^{II}	Octahedral (Ga)	4.73	d-Chloroform; 25 °C; 500 MHz	53
Ga^{III}–(OH)–Sr^{II}	Octahedral (Ga)	4.49	d-Chloroform; 25 °C; 500 MHz	53

Table 5 ^{1}H NMR data for μ_3-OH bridges linking homometallic atoms

Metal	Molecular geometry of M^{X+}	μ_3-OH Chem. shift (ppm)	NMR conditions	Ref.
Ca^{II}	Octahedral	1.32, 2.77, 4.57	d_6-Benzene; 25 °C; 300 MHz	44
Rh^I	Six coordinate^a	−1.05	d_4-Methanol; 300 MHz	54
Rh^I	Six coordinate^a	−0.61, −0.48, −0.02	d_2-Dichloromethane; 300 MHz	54
Sn^{IV}	Trigonal bipyramidal	3.219, 3.221	d-Chloroform; 500 MHz	55
Th^{IV}	Square pyramidal^b	5.97, 6.16, 6.79	d_6-DMSO; 500 MHz	56
Y^{III}	Dodecahedral^c	2.93, 3.1	d_3-Acetonitrile; 300 MHz	57
Y^{III}	Dodecahedral	6.05	d_3-Acetonitrile	58
Zn^{II}	Trig. bipyramidal/octahedral	5.4	d-Chloroform; 25 °C; 300 MHz	59

^{a} No indication of molecular geometry. ^{b} Distorted geometry. ^{c} Associated CuI$_3{}^{2-}$.

ranges observed for "trivalent octahedral" metal complexes. In addition to experimental data, computational data is occasionally found for bridging hydroxides. For instance, computed ^{1}H-NMR shifts during the oligomerization of Be(II) species mirrors the experimental measurement of 4.3 ppm.[22,23] Like the trivalent octahedral complexes listed above, certain metals have distinct areas within the bigger region were the ^{1}H-NMR signals of μ_2-OH bridges appear. The data presented in the bottom

section of Table 3 reveals these ranges. As previously mentioned, octahedral Co(III) complexes differ from the other trivalent octahedral complexes with signals appearing between −4.5 and 0.5 ppm.[17–21] Mixed valence Os(0/II) compounds tend to have bridges in the −2.8 to −0.44 ppm range.[24,25] Square planar Pd(II) and Pt(II) complexes have μ_2-OH bridges that range from −3 to 2 ppm.[26–34] Sn has the largest range producing signals anywhere from 1.63 to 7.33 ppm.[35–39] Yttrium hydroxo bridges tend to have chemical shift values downfield ranging
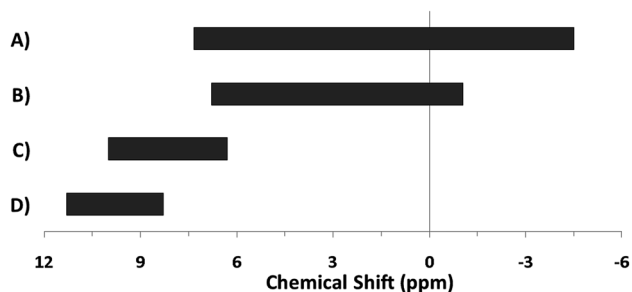

Fig. 2 General ^{1}H-NMR signal regions for bridging hydroxides and aquo ligands in all metal complexes surveyed. (A) μ_2-OH bridges (−4.5 to 7 ppm); (B) μ_3-OH bridges (−1.05 to 6.79 ppm); (C) aquo ligands in multimetallic complexes (6.3–10 ppm); (D) hexaquo metal complexes (8.3–11.3 ppm).
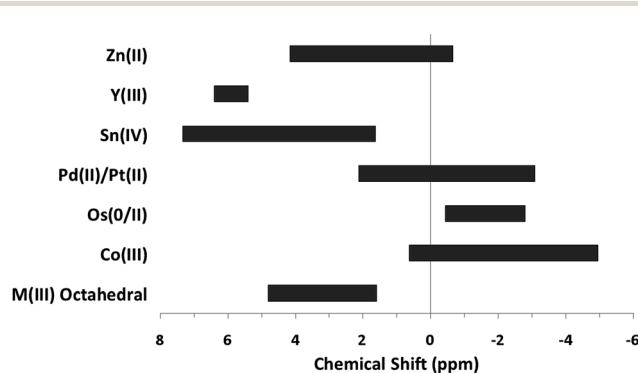

Fig. 3 General ^{1}H-NMR signal regions for homometallic μ_2-OH bridges in a variety of metal complexes.

from 5.2 to 6.4 ppm.[40] Zn(II) bridges fall into the −1.15 to 4.16 range.[41–43] The proton signal for the only example of a Cd–(μ_2-OH)–Cd bridge appeared at −2.43 ppm.[42] The typical ranges of these metal hydroxo bridges have been plotted in Fig. 3 to allow for easy comparison.

Data from the literature for heterometallic complexes was also analysed because the present work focuses on hetero-metallic Ga/In clusters as well. Not all of the heterometallic complexes in Table 4 feature bridging hydroxides between two different metal atoms, but for completeness they were included.

The hydroxo bridges in trivalent Group 13 octahedral metal complexes are the most relevant for this report. Akitt and colleagues suggests a range of 3 to 6 ppm for Al^{3+} μ_2-OH bridges.[3] However, the data listed above suggests these reso-nances should fall within the 2.0 to 4.8 ppm region. The het-erometallic octahedral Ga–(μ_2-OH)–M (M ≠ Ga) bridges have very similar chemical shifts to the homometallic hydroxo bridges listed in Table 2. This indicates that Ga–(μ_2-OH)–Ga bridges may not easily be distinguished from Ga–(μ_2-OH)–In bridges. Fig. 4 illustrates the regions where μ_2-OH bridges and capping water ligands on the $Ga_{13-x}In_x$ clusters most likely will resonate.

One trend that stood out in the general data was that hydroxide bridges shift downfield with increased coordination number of the metal. This trend is visible with metals such as Sn, Ga, and Zr (Fig. 5). These were the only metals that had data from several independent sources allowing reasonable

conclusions to be made. This trend holds true for all of Group 13, not just gallium (Fig. 6). Tetrahedral gallium has a Ga–(μ_2-OH)–Ga bridge at 0.14 ppm,[50] Square pyramidal gallium and indium have peaks in the 1 to 1.5 ppm range,[51,60] and as stated above octahedral aluminium and gallium produce signals between 2 and 5 ppm.

^{1}H-NMR data reported for μ_3-OH protons are even scarcer. As previously stated, these signals appear from −1.05 to 6.79 ppm. The proton chemical shifts in these complexes are listed in Table 5. No examples of Group 13 metals with μ_3-OH ligands were found. The most relevant is the trivalent yttrium complex with a proton signal at 6.05 ppm.[58] Related hydroxide ligands in Th(IV) and Zn(II) compounds also resonate in this region.[56,59] Unfortunately, there are not enough examples of μ_3-OH protons to suggest any trends or regions for specific metals or coordi-nation geometries.

This brief literature survey will not only help the structural study and assignments presented herein, but we hope this serves as a useful resource for others seeking to assign aquo and bridging hydroxo ligands in inorganic clusters and related compounds. This survey highlights some of the challenges in interpreting even the most basic NMR signals. For example, when two distinct μ_2-OH signals arise in the same ^{1}H-NMR spectrum, it can be difficult to tell them apart. Two examples of this from above are the Al–(μ_2-OH)–Al bridges of Elders and colleagues' Keggin cluster,[7] and the hexanuclear yttrium species by Hubert-Pfalzgraf and coworkers.[57]

These data can also help with identifying possibly mis-assigned signals. For instance, in [Al(μ-OH)(hbo)$_2$]$_2$ (hbo: 2-(2′-hydroxphenyl)-2-benzoxazole) a peak at 11.47 ppm observed in CDCl$_3$ is proposed to be the bridging hydroxo ligands.[61] Is it possible that this is really a small amount of an aquo–Al(III) complex or some other aquo ligand-containing species? The data reported herein and our literature survey suggest that resonances this far downfield are typically due to aquo ligands; however, there are very few examples of NMR data reported for such species in CDCl$_3$, so much remains to be learned. Simi-larly, are the peaks assigned to aquo ligands in the spectra of Al(III) and Ga(III) porphyrins containing Ga–(μ_2-OH)–Ga and In–(μ_2-OH)–In bridges at 1.5 and 1.56 ppm, respectively, actu-ally the hydroxide bridges?[60] Hopefully, these tabulated data can be helpful for the future assignment of μ_2-OH and μ_3-OH bridges in related compounds and help begin to develop a reliable database of such peak assignments.
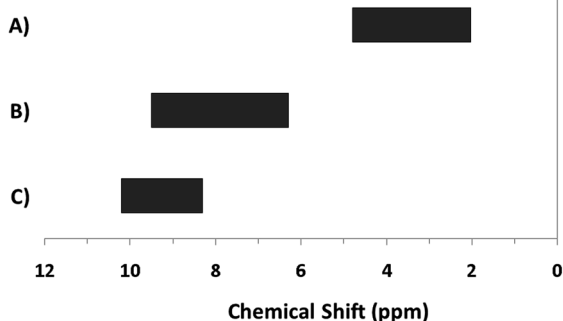

Fig. 4 General ^{1}H-NMR signal regions for hydroxo bridges and aquo ligands on Group 13 metals. (A) μ_2-OH ligands; (B) aquo ligands in multimetallic complexes; (C) hexaaquo metal complexes.
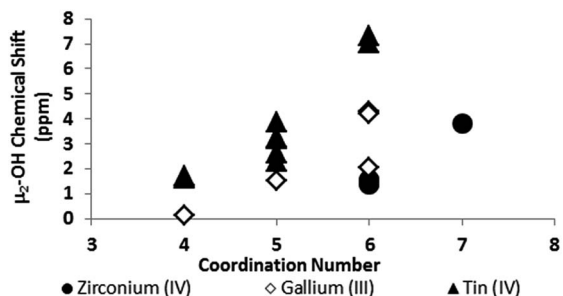

Fig. 5 As the coordination number of a cation increases, the ^{1}H-NMR signals shift downfield (Tables 2 and 3).
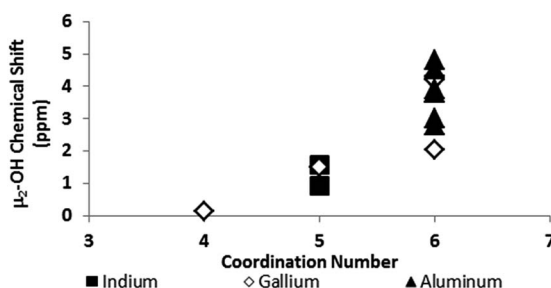

Fig. 6 As the coordination number in Group 13 increases, the ^{1}H-NMR signals shift downfield (Tables 2 and 3).

Experimental section

Chemicals were purchased from Sigma-Aldrich, TCI America, and STREM, and were used as received without further purification. The $Ga_{13-x}In_x$ clusters were synthesized using previously published methods.[13,15,62] ^{1}H-NMR experiments were conducted at 25 °C in 5 mm tubes on a 500 MHz Varian spectrometer. Data were collected using Varian Software, referenced to TMS, and processed using MestReNova. The DOSY experiments were performed using the gradient stimulated echo with spin-lock and convection compensation (DgsteSL_cc) pulse sequences. All Varian software standard default settings were kept for DOSY unless otherwise stated. The diffusion delay was increased to 200 ms, the number of increments was increased to 20, and the highest gradient value was set to 25 000. The alternate gradient sign on odd scans and lock gating during gradient portions were also selected. All Varian software standard default settings were kept for NOESY unless otherwise stated. The NOESY experiment was performed after setting the 90° pulse-width to 13.0 ms, d scale increment to 700 ms, and the t_1 increment to 256. To acquire quality resolution, 16 scans were performed.

Quantum mechanical computations were used to predict the chemical shifts of each hydroxo proton in the clusters. The geometries of all of the clusters were obtained from the crystal structures, including the counterions. The NMR chemical shifts were computed using gauge-independent atomic orbital (GIAO) method in B3LYP/def2-SVP level of theory in the gas-phase, all as implemented in Gaussian03.[63] Since the position of the

counterions was not perfectly symmetric, we computed the chemical shifts for multiple counterion positions for each cluster structure, in order to eliminate the effects of static, individual counterion positions on the proton shifts. For example, for Ga_8In_5, with one external gallium, we computed the chemical shifts of 6 geometries of this cluster, one for each position the gallium could occupy relative to the counterion positions. Each computed shift for each type of proton was averaged across clusters of the same geometry discounting counterions, and the shifts were scaled using constant factors for each type.[16]

This particular method and procedure were chosen because exclusion of the counterions yielded incorrect ordering of the external and internal μ_2-OH protons, regardless of geometry of
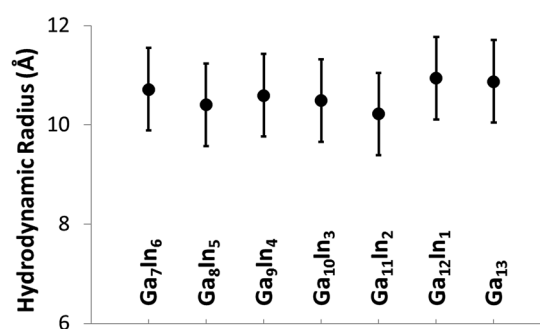

Fig. 8 Hydrodynamic radii and standard deviation of the clusters measured via DOSY.

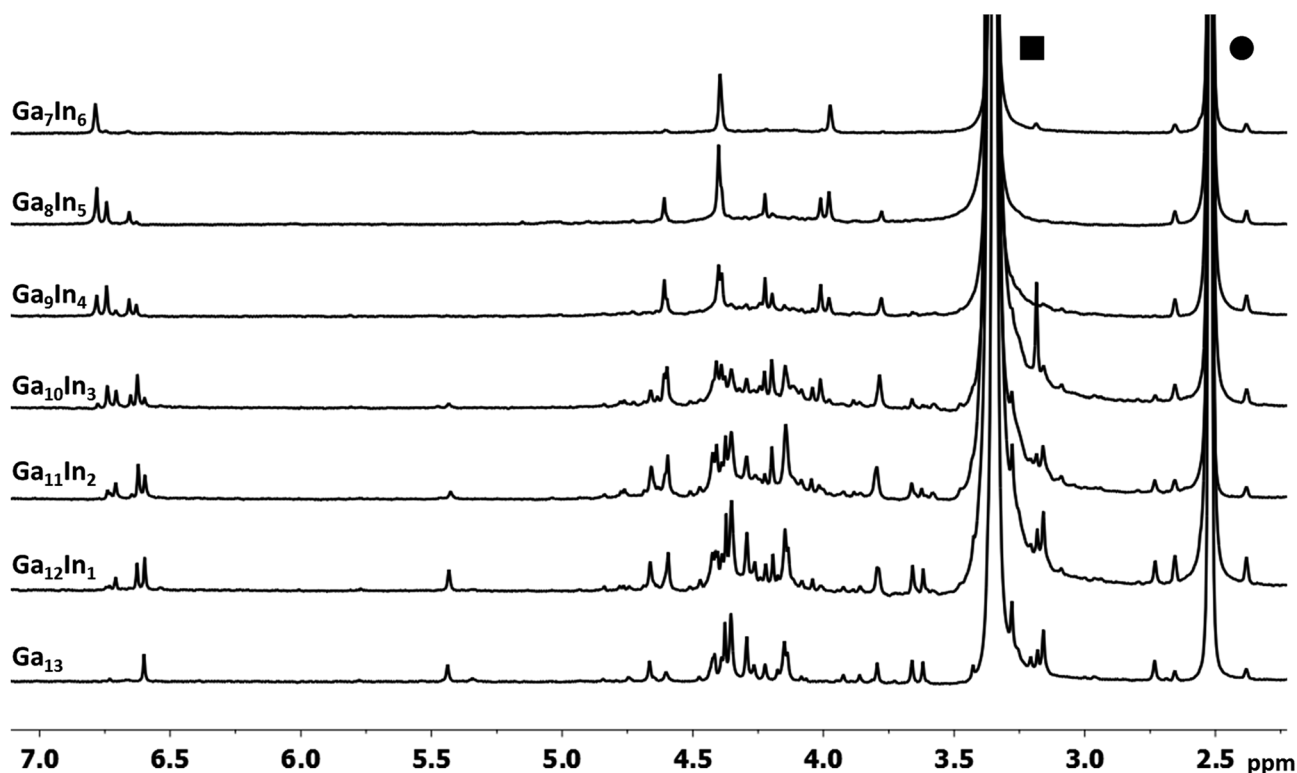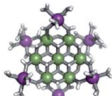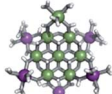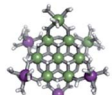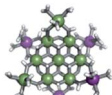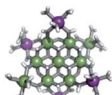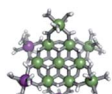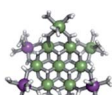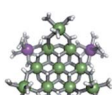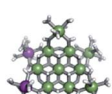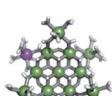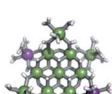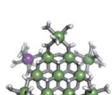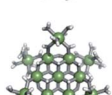Fig. 7 ^{1}H-NMR spectra of 2 mM clusters in d_6-DMSO one day after dissolution. H_2O peak (■) and DMSO peak (●).

Table 6 The symmetry and expected proton signal ratios for each type of hydroxide for all studied $Ga_{13-x}In_x$ clusters

Cluster	# of isomers	Structure	Point group	Expected signals		
				6 μ_3-OH	6 μ_2-OH$_{int}$	12 μ_2-OH$_{ext}$
Ga_7In_6	1		D_{3d}	$6H^{\mu_3}_{InInIn}$(A)	$6H^{\mu_{2int}}_{InInIn}$(G)	$12H^{\mu_{2ext}}_{InIn}$(M)
Ga_8In_5	1		C_{2v}	$3H^{\mu_3}_{InInIn}$(A) $2H^{\mu_3}_{InInGa}$(B) $1H^{\mu_3}_{InGaIn}$(D)	$3H^{\mu_{2int}}_{InInIn}$(G) $2H^{\mu_{2int}}_{InInGa}$(H) $1H^{\mu_{2int}}_{InGaIn}$(J)	$8H^{\mu_{2ext}}_{InIn}$(M) $2H^{\mu_{2ext}}_{InGa}$(N) $2H^{\mu_{2ext}}_{GaIn}$(O)
Ga_9In_4	3		C_{2v}	$2H^{\mu_3}_{InInIn}$(A) $2H^{\mu_3}_{InInGa}$(B) $2H^{\mu_3}_{GaGaIn}$(E)	$2H^{\mu_{2int}}_{InInIn}$(G) $2H^{\mu_{2int}}_{InInGa}$(H) $2H^{\mu_{2int}}_{GaGaIn}$(K)	$6H^{\mu_{2ext}}_{InIn}$(M) $2H^{\mu_{2ext}}_{InGa}$(N) $2H^{\mu_{2ext}}_{GaIn}$(O) $2H^{\mu_{2ext}}_{GaGa}$(P)
			C_{2v}	$1H^{\mu_3}_{InInIn}$(A) $2H^{\mu_3}_{InInGa}$(B) $1H^{\mu_3}_{GaInIn}$(C) $2H^{\mu_3}_{InGaIn}$(D)	$1H^{\mu_{2int}}_{InInIn}$(G) $2H^{\mu_{2int}}_{InInGa}$(H) $1H^{\mu_{2int}}_{GaInGa}$(I) $2H^{\mu_{2int}}_{InGaIn}$(J)	$4H^{\mu_{2ext}}_{InIn}$(M) $4H^{\mu_{2ext}}_{InGa}$(N) $4H^{\mu_{2ext}}_{GaIn}$(O)
			C_{2v}	$4H^{\mu_3}_{InInGa}$(B) $2H^{\mu_3}_{InGaIn}$(D)	$4H^{\mu_{2int}}_{InInGa}$(H) $2H^{\mu_{2int}}_{InGaIn}$(J)	$4H^{\mu_{2ext}}_{InIn}$(M) $4H^{\mu_{2ext}}_{InGa}$(N) $4H^{\mu_{2ext}}_{GaIn}$(O)
$Ga_{10}In_3$	3		C_{2v}	$1H^{\mu_3}_{InInIn}$(A) $2H^{\mu_3}_{InInGa}$(B) $2H^{\mu_3}_{GaGaIn}$(E) $1H^{\mu_3}_{GaGaGa}$(F)	$2H^{\mu_{2int}}_{InInIn}$(G) $2H^{\mu_{2int}}_{InInGa}$(H) $2H^{\mu_{2int}}_{GaGaIn}$(K) $3H^{\mu_{2int}}_{GaGaGa}$(L)	$4H^{\mu_{2ext}}_{InIn}$(M) $2H^{\mu_{2ext}}_{InGa}$(N) $2H^{\mu_{2ext}}_{GaIn}$(O) $4H^{\mu_{2ext}}_{GaGa}$(P)
			C_1	$2H^{\mu_3}_{InInGa}$(B) $1H^{\mu_3}_{GaInGa}$(C) $1H^{\mu_3}_{InGaIn}$(D) $2H^{\mu_3}_{GaGaIn}$(E)	$2H^{\mu_{2int}}_{InInGa}$(H) $1H^{\mu_{2int}}_{GaInGa}$(I) $1H^{\mu_{2int}}_{InGaIn}$(J) $2H^{\mu_{2int}}_{GaGaIn}$(K)	$2H^{\mu_{2ext}}_{InIn}$(M) $4H^{\mu_{2ext}}_{InGa}$(N) $4H^{\mu_{2ext}}_{GaIn}$(O) $2H^{\mu_{2ext}}_{GaGa}$(P)
			C_{3v}	$3H^{\mu_3}_{GaInGa}$(C) $3H^{\mu_3}_{InGaIn}$(D)	$3H^{\mu_{2int}}_{GaInGa}$(I) $3H^{\mu_{2int}}_{InGaIn}$(J)	$6H^{\mu_{2ext}}_{InGa}$(N) $6H^{\mu_{2ext}}_{GaIn}$(O)
$Ga_{11}In_2$	3		C_{2v}	$2H^{\mu_3}_{InInGa}$(B) $2H^{\mu_3}_{GaGaIn}$(E) $2H^{\mu_3}_{GaGaGa}$(F)	$2H^{\mu_{2int}}_{InInGa}$(H) $2H^{\mu_{2int}}_{GaGaIn}$(K) $2H^{\mu_{2int}}_{GaGaGa}$(L)	$2H^{\mu_{2ext}}_{InIn}$(M) $2H^{\mu_{2ext}}_{InGa}$(N) $2H^{\mu_{2ext}}_{GaIn}$(O) $6H^{\mu_{2ext}}_{GaGa}$(P)
			C_{2v}	$2H^{\mu_3}_{GaInGa}$(C) $1H^{\mu_3}_{InGaIn}$(D) $2H^{\mu_3}_{GaGaIn}$(E) $1H^{\mu_3}_{GaGaGa}$(F)	$2H^{\mu_{2int}}_{GaInGa}$(I) $1H^{\mu_{2int}}_{InGaIn}$(J) $2H^{\mu_{2int}}_{GaGaIn}$(K) $1H^{\mu_{2int}}_{GaGaGa}$(L)	$4H^{\mu_{2ext}}_{InGa}$(N) $4H^{\mu_{2ext}}_{GaIn}$(O) $4H^{\mu_{2ext}}_{GaGa}$(P)
			C_{2v}	$2H^{\mu_3}_{GaInGa}$(C) $4H^{\mu_3}_{GaGaIn}$(E)	$2H^{\mu_{2int}}_{GaInGa}$(I) $4H^{\mu_{2int}}_{GaGaIn}$(K)	$4H^{\mu_{2ext}}_{InGa}$(N) $4H^{\mu_{2ext}}_{GaIn}$(O) $4H^{\mu_{2ext}}_{GaGa}$(P)
$Ga_{12}In_1$	1		C_{2v}	$1H^{\mu_3}_{GaInGa}$(C) $2H^{\mu_3}_{GaGaIn}$(E) $3H^{\mu_3}_{GaGaGa}$(F)	$1H^{\mu_{2int}}_{GaInGa}$(I) $2H^{\mu_{2int}}_{GaGaIn}$(K) $3H^{\mu_{2int}}_{GaGaGa}$(L)	$2H^{\mu_{2ext}}_{InGa}$(N) $2H^{\mu_{2ext}}_{GaIn}$(O) $8H^{\mu_{2ext}}_{GaGa}$(P)
Ga_{13}	1		D_{3d}	$6H^{\mu_3}_{GaGaGa}$(F)	$6H^{\mu_{2int}}_{GaGaGa}$(L)	$12H^{\mu_{2ext}}_{GaGa}$(P)

the protons at any level of theory attempted by our hands. Initially, we fully optimized the entire cluster species, including the proton positions. However, the resulting structures deviated largely from the known symmetry of these structures as determined by NMR, yielding wildly varying values for the chemical shifts of identical proton types. In addition, it is important to note that the theoretical predictions of the proton spectra appeared uncannily consistent with experimental spectra, even with accounting for all peaks. However, upon deeper examination of the experimental spectra of the clusters, we have discovered that the internal and external μ_2-OH signals were switched (see ESI†). Therefore, these were not used, and crystallographically determined positions were used instead. Bond lengths for the oxygen hydrogen bonds determined from crystallography may often be 0.2–0.3 Å short; however, we found that experimentally consistent and useful computed shift values could still be obtained in comparison to experiments, in contrast to results from DFT geometry optimizations.

Results and discussion

The mixed $Ga_{13-x}In_x$ clusters each yield a unique ^{1}H-NMR spectrum after one day in d_6-DMSO solution (Fig. 7).[64] The clusters were crystallographically resolved prior to ^{1}H-NMR analysis to determine the stoichiometric ratio of the metal atoms. Diffusion Ordered Spectroscopy (DOSY) was used to verify the presence and integrity of clusters in solution (see ESI Fig. SI1–7†). The hydrodynamic radius of each heterometallic cluster matches that of Ga_{13} (Fig. 8), which was previously characterized using complementary techniques.[2,65] The combination of consistent hydrodynamic radii and the absence of any other proton signals (other than solvent) suggest that the spectra of the clusters consist of bridging hydroxide and/or capping water ligand signals. The distinct combinations of resonances observed in each spectrum confirm that the heterometallic clusters exist as distinct species.

Understanding the symmetry of these $Ga_{13-x}In_x$ clusters is essential for analyzing and assigning the proton shifts from NMR. The symmetry of each cluster dictates the number of expected signals that the cluster will have from the hydroxyl protons and aquo ligands. For example, the Ga_7In_6 and Ga_{13} clusters have identical symmetry, and therefore should only ideally yield three total signals from hydroxyl protons. Table 6 lists the symmetry of all $Ga_{13-x}In_x$ clusters studied herein.

Water ligands coordinated to multimetallic Group 13 complexes are known to produce signals from 7–10 ppm.[3] The $Ga_{13-x}In_x$ clusters contain signals between 2.5 and 7 ppm, which falls into the range expected for μ_2-OH and μ_3-OH bridges. The spectrum of Ga_7In_6 is much simpler than that of the Ga_{13} cluster.[2] We suspect this is due to the fact that the 1st order rate constant of water exchange for In(III) is 100× faster than for Ga(III) (4×10^4 s^{-1} and 4×10^2 s^{-1}, respectively).[66] The lack of peaks in the 7–10 ppm region indicates that the exchange rate of the outer water ligands is too fast to observe on the NMR time scale.[2] The rapid aquo ligand exchange of the In(III) ions allows us to observe only the protons associated with the central 7-atom Ga(III) core of Ga_7In_6 leading to 3 signals

(μ_3-OH, μ_2-OH$_{ext}$, and μ_2-OH$_{int}$) are observable. This aquo ligand exchange process happens much slower with gallium; therefore, the symmetry within the core of Ga_{13} is not retained and results in a complex spectrum containing more proton signals.

1. Ga_7In_6 peak assignments: establishing a basis for comparison

Ga_7In_6 is a great test case to understand the more complicated clusters where gallium occupies one or more of the peripheral metal sites. The simplicity of the experimental data and the high symmetry of this cluster makes this cluster ideal for the purpose of assigning regions of the spectrum to particular types of protons, which in turn may be used to assign shifts for the other clusters. This assignment was in turn used to determine an appropriate computational method for predicting the proton shifts of the remaining clusters. The computations resulted in subtle differences in the positions of the signals from different types of hydroxo bridges in the clusters, in particular, the μ_2-OH region, which shows strong overlap of the two types of signals (Fig. 7). The μ_3-OH proton signals are observed between 6.5 and 7.0 ppm. The remaining μ_2-OH$_{int}$ and μ_2-OH$_{ext}$ proton signals are found between 3.5 and 5.0 ppm.

Ga_7In_6 ^{1}H-NMR spectra reveal 3 signals, which can be assigned to the three types of bridging hydroxides (Fig. 9). These three signals integrate to a 1 : 2 : 1 ratio, matching the number of protons on specific hydroxide bridges within the 7-atom cluster core (μ_3-OH : μ_2-OH$_{ext}$: μ_2-OH$_{int}$ ratio = 6 : 12 : 6) (Fig. 1, Table 6). This suggests that the peak at 4.4 ppm corresponds to the μ_2-OH$_{ext}$, which bridge between the 7-atom gallium core and the exterior indiums ions. Other examples of mixed metal Ga–(μ_2-OH)–M bridges corroborate this assignment (Ga–(μ_2-OH)–Ca and Ga–(μ_2-OH)–Sr; 4.73 ppm and 4.49 ppm respectively).[53] As stated above, the signal furthest downfield (~6.8 ppm) corresponds to the protons of the μ_3-OH, similar to the chemical shift of the μ_3-OH bridge in the octahedral Y^{3+} complex.[58] The final peak at 4.0 ppm represents the μ_2-OH$_{int}$ protons. This assignment is in agreement with M–(μ_2-OH)–M bridges reported for other Group 13 complexes.[5,7–10]

Due to the simplicity of Ga_7In_6, the spectra and analysis for this cluster make a good basis for determining a suitable theoretical method for computational elucidation of the μ_2-OH signals. Most importantly, computations performed without explicit counterions in the structure predict the exact opposite
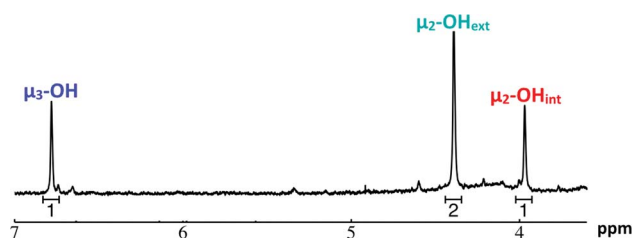

Fig. 9 ^{1}H-NMR spectra of 2 mM Ga_7In_6 cluster in d_6-DMSO one day after dissolution: the visible signals correspond to the 3 types of bridging hydroxides.
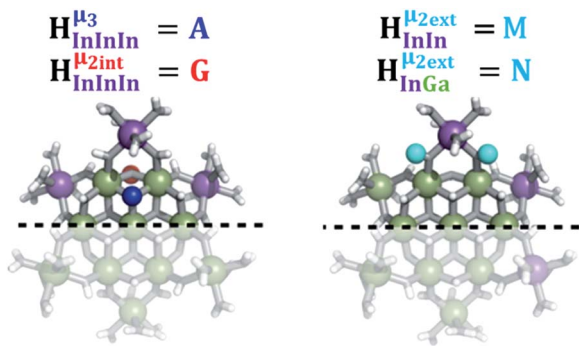
$H^{\mu_3}_{InInIn} = A$
$H^{\mu_{2int}}_{InInIn} = G$
$H^{\mu_{2ext}}_{InIn} = M$
$H^{\mu_{2ext}}_{InGa} = N$

Fig. 10 Naming system for protons in the $Ga_{13-x}In_x$ clusters.

ordering of the internal and external μ_2-OH signals. This was so, regardless of the theoretical methods (HF, B3LYP), basis sets (6-31G*[67,68]/LANL2DZ,[69,70] def2-SVP,[71] def2-TZVP,[71] def2-QZVP,[71] etc.), or solvation methods (gas, COSMO,[72] PCM,[73] and CPCM[74]) employed. From our observations, improvements in levels of theory are unlikely to address the discrepancy. However, when counterions are included, correct ordering is obtained, namely that the μ_2-OH$_{ext}$ signals are downfield from the μ_2-OH$_{int}$ protons (Fig. 9). These results indicate that the presence, location, and identity of the counterions is immensely important for determining even the qualitative assignments of ^{1}H-NMR chemical shifts of aqueous metal clusters. The ordering or the μ_2-OH$_{int}$ and μ_2-OH$_{ext}$ protons is more difficult to see for the

remainder of the clusters due to significant overlap of μ_2-OH signals, and computations were diagnostic in discriminating these convoluted overlapping signals in all the clusters.

2. Hydroxo ligand naming convention

As gallium is substituted for indium in the exterior positions of the cluster, a greater number of proton types emerge (Fig. 6). There are 16 unique types of protons in the clusters based on idealized symmetry: 6 μ_3-OH, 6 μ_2-OH$_{int}$, and 4 types of μ_2-OH$_{ext}$ (Table 6). The environments of these protons were determined by the identity of the nearest external metal ion and its two nearest neighbors (i.e., Ga or In). For example, proton $H^{\mu_3}_{InInIn}$ is a μ_3-OH proton in a section of the cluster with an exterior indium ion directly outside (always indicated in bold) possessing two additional exterior indium atoms on either side (Fig. 10). Proton $H^{\mu_{2int}}_{InInIn}$ corresponds to the symmetry-equivalent μ_2-OH$_{int}$ proton bridging the same metals as proton $H^{\mu_3}_{InInIn}$ (Fig. 10). The μ_2-OH$_{ext}$ protons are described in a similar manner. Proton $H^{\mu_{2ext}}_{InIn}$ corresponds to the μ_2-OH$_{ext}$ proton connected to an indium ion (indicated in bold) and positioned facing towards a second indium. This naming system is comprehensively represented by Table 6.

3. μ_3-OH peak assignments

The peak in the 6.55–6.85 ppm region of the Ga_7In_6 spectrum corresponds to the μ_3-OH protons. This region contains the

Table 7 Unique μ_3-OH proton environments of each cluster and the corresponding ^{1}H-NMR fingerprint region (*assuming 1 : 1 : 1 isomeric ratio)

Corresponding μ_3-OH NMR spectra (ppm)	Cluster	Expected proton ratios (observed proton ratios)						# of isomers
		$H^{\mu_3}_{InInIn}$	$H^{\mu_3}_{InInGa}$	$H^{\mu_3}_{GaInGa}$	$H^{\mu_3}_{InGaIn}$	$H^{\mu_3}_{GaGaIn}$	$H^{\mu_3}_{GaGaGa}$	
	Ga_7In_6	6 (6)	—	—	—	—	—	1
	Ga_8In_5	3 (3)	2 (2)	—	1 (1)	—	—	1
	Ga_9In_4	3 (4)	8 (6)	1 (1)	4 (3)	2 (2)	—	3*
	$Ga_{10}In_3$	1 (1)	4 (6)	4 (3)	4 (3)	4 (6)	1 (1)	3*
	$Ga_{11}In_2$	—	2 (2)	4 (3)	1 (1)	8 (6)	3 (4)	3*
	$Ga_{12}In_1$	—	—	1 (1)	—	2 (2)	3 (3)	1
	Ga_{13}	—	—	—	—	—	6 (6)	1

6.85 6.80 6.75 6.70 6.65 6.60 6.55 6.50

simplest set of signals in all the mixed clusters. We suspect that this is because the μ_3-OH protons are the farthest away from, and therefore, the least affected by the bound DMSO. Each peak in this region for the 7 NMR spectra is corresponds to one of the 6 types of μ_3-OH protons (Table 7). Proximity to the indium ion causes downfield shifting in the proton signal. This is best shown in **Ga$_7$In$_6$**, which has one type of proton ($H^{\mu_3}_{InInIn}$), and exhibits the farthest downfield signal. **Ga$_{13}$** also has only one type of μ_3-OH proton ($H^{\mu_3}_{GaGaGa}$); however, the lack of indium atoms in the structure leads to the farthest upfield μ_3-OH signal. **Ga$_8$In$_5$** and **Ga$_{12}$In$_1$** each possess one isomer and 3 unique μ_3-OH proton types ($H^{\mu_3}_{InInIn}$, $H^{\mu_3}_{InInGa}$, $H^{\mu_3}_{InGaIn}$ and $H^{\mu_3}_{GaGaGa}$, $H^{\mu_3}_{GaGaIn}$, $H^{\mu_3}_{GaInGa}$, respectively) in 3 : 2 : 1 ratios. This is mirrored in the NMR spectra facilitating the assignment of each proton type to a peak (Table 7). **Ga$_9$In$_4$**, **Ga$_{10}$In$_3$**, and **Ga$_{11}$In$_2$** are slightly more complicated because each has 3 possible isomers (Table 6), but each predicted μ_3-OH peak is observed. The $H^{\mu_3}_{InInIn}$ type protons are shifted farthest downfield, while the $H^{\mu_3}_{GaGaGa}$ type protons are shifted the farthest upfield, for an overall ranking from highest to lowest ppm of $H^{\mu_3}_{InInIn} > H^{\mu_3}_{InInGa} > H^{\mu_3}_{GaInGa} > H^{\mu_3}_{InGaIn} > H^{\mu_3}_{GaGaIn} > H^{\mu_3}_{GaGaGa}$ (Table 7). Computations support that these signals are produced by μ_3-OH protons and that the $H^{\mu_3}_{InInIn}$,
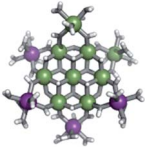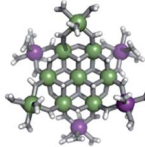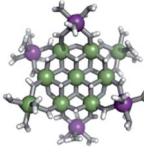
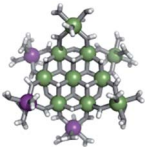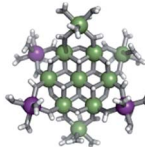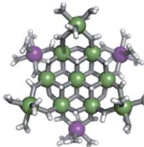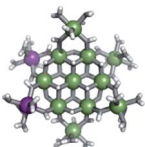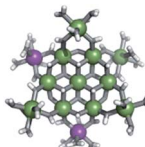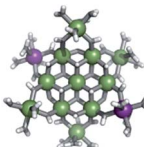$H^{\mu_3}_{InInGa}$, and $H^{\mu_3}_{InGaIn}$ protons should be more deshielded than the $H^{\mu_3}_{InGaIn}$, $H^{\mu_3}_{GaGaIn}$, and $H^{\mu_3}_{GaGaGa}$ protons. The calculations cannot corroborate or contradict the relative rankings within those two sets (Table 7).

In the case of clusters with multiple isomers, the peak integrations of the μ_3-OH protons in the NMRs can provide information about the ratio of each isomer present in the sample. The statistical probability of each isomer, along with the calculated % present in solution, is shown in Table 8. Similarities in the structures of **Ga$_9$In$_4$** and **Ga$_{11}$In$_2$** allow for comparisons.[75] The NMR data remarkably show a strong correlation to the statistical ratio of isomeric heterometallic clusters. This data indicates that no specific substitution pattern of indium in the outer shell of the clusters is kinetically favorable.

4. μ_2-OH peak assignments

The μ_2-OH regions of the NMR spectra are not as easily deconvoluted. Based on the **Ga$_7$In$_6$** spectrum, the upfield peaks correspond to μ_2-OH bridges, but as more gallium atoms are introduced into the outermost shell and exchange between the coordinating water ligands and DMSO slows, symmetry is broken, and complexity increases. We now propose to assign

Table 8 The isomers of Ga$_9$In$_4$, Ga$_{10}$In$_3$, and Ga$_{11}$In$_2$ with relative μ_2-OH peak intensities predicted using the integration of μ_3-OH protons, ratio of isomers in solution based on probability, and experimental percentage of isomers present in solution calculated using the μ_3-OH proton integrations. Green: gallium. Purple: indium

Protons	$H^{\mu_2int}_{InInIn}$ (G)	$H^{\mu_2int}_{InInGa}$ (H)	$H^{\mu_2int}_{GaInGa}$ (I)	$H^{\mu_2int}_{InGaIn}$ (J)	$H^{\mu_2int}_{GaGaIn}$ (K)	$H^{\mu_2int}_{GaGaGa}$ (L)	$H^{\mu_2ext}_{InIn}$ (M)	$H^{\mu_2ext}_{InGa}$ (N)	$H^{\mu_2ext}_{InGa}$ (O)	$H^{\mu_2ext}_{GaGa}$ (P)
Integrations	4	6	1	3	2	—	12	8	8	2
Ga$_9$In$_4$ Isomers										
Experimental		40%			40%				20%	
Probability		40%			40%				20%	
Integrations	1	6	3	3	6	1	8	13	13	8
Ga$_{10}$In$_3$ isomers										
Experimental		40%			50%				10%	
Probability		30%			60%				10%	
Integrations	—	2	3	1	6	4	2	8	8	12
Ga$_{11}$In$_2$ isomers										
Experimental		—			—				—	
Probability		40%			40%				20%	

these peaks as well. As with the μ_3-OH protons, computations were used to establish the range in which the μ_2-OH protons should be found.

4.1 Ga_8In_5. After the Ga_7In_6 cluster, Ga_8In_5 is the next easiest to analyze because it only has one isomer. Using the information gained in the μ_3-OH assignment a similar analysis involving integrations of signals and protons signals can be assigned (Fig. 11). The μ_2-OH$_{int}$ are the same as their μ_3-OH counterparts existing in a 3 : 2 : 1 ratio ($H_{InInIn}^{\mu_2int}$: $H_{InInGa}^{\mu_2int}$: $H_{InGaIn}^{\mu_2int}$). The μ_2-OH$_{ext}$ appear in an 8 : 2 : 2 ratio ($H_{InIn}^{\mu_2ext}$: $H_{InGa}^{\mu_2ext}$: $H_{GaIn}^{\mu_2ext}$), making it difficult to differentiate between protons $H_{InGa}^{\mu_2ext}$ and $H_{GaIn}^{\mu_2ext}$. However, Nuclear Overhauser Effect Spectroscopy (NOESY) correlates protons that are near each other through space. The μ_3-OH protons are 3.34 Å and 3.24 Å away from the neighboring μ_2-OH$_{ext}$ bridges in the solid state. Since the μ_3-OH and μ_2-OH$_{ext}$ bridges are significantly less than 5 Å,[76] they exhibit strong through-space interactions allowing $H_{InGa}^{\mu_2ext}$ and $H_{GaIn}^{\mu_2ext}$ to be assigned using NOESY (Fig. 12).

The use of these experimental results allowed for additional verification of quantum mechanical methods. The assignments based on integration values and the NOESY spectra established
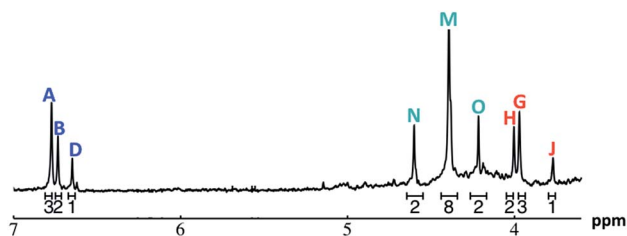
a basis of comparison for determining the most accurate computational method. Using the average computed NMR shifts from the structures with counterions for each proton type, the computed results were compared to the experimentally determined proton shifts for several basis sets, as mentioned previously. The def2-SVP basis set was found to provide the optimal combination of accuracy and computational time, as the computed proton rankings were an exact match with experimental results. Therefore, we know this computational method can be used to assign the protons in the more complicated spectra with a larger number of isomers and an increasing number of gallium centers.

4.2 Ga_9In_4. Ideally Ga_9In_4 has 5 types of μ_2-OH$_{int}$ and all 4 types of μ_2-OH$_{ext}$ bridges. As previously stated, this cluster has 3 isomers which exist in a 2 : 2 : 1 ratio. This means that the protons in Ga_9In_4 integrate to the ratios shown in Table 8. Based on these integrations, peaks have been experimentally assigned to the Ga_9In_4 spectrum (Fig. 13). Peaks $H_{InInIn}^{\mu_2int}$, $H_{InInGa}^{\mu_2int}$, and $H_{InGa}^{\mu_2ext}$ are the same as for Ga_8In_5. Proton $H_{GaInGa}^{\mu_2int}$ which integrates to 1 is too small to identify in the baseline noise between 3.7 and 4.8 ppm. The peak for proton $H_{InGaIn}^{\mu_2int}$ overlaps with $H_{GaGaIn}^{\mu_2int}$ giving an integration of 5 for the combined signal. There should still be a strong signal at 4.4 ppm from $H_{InIn}^{\mu_2ext}$ for Ga_9In_4; however, an integration of 14 suggests that proton $H_{GaGa}^{\mu_2ext}$ also appears at this chemical shift. Interestingly, the signal for proton $H_{GaIn}^{\mu_2ext}$ seems to have split into two peaks at ~4.2 ppm. This is most likely due to the slower exchange rate of the outer water ligands on gallium. Because $H_{GaIn}^{\mu_2ext}$ is bridging an outer gallium atom this may be the first sign of the complex spectrum we see for Ga_{13}. This may also explain the small shoulder/splitting of peak $H_{InGa}^{\mu_2ext}$ and $H_{InIn}^{\mu_2ext}$/$H_{GaGa}^{\mu_2ext}$.

Computations are particularly useful for corroborating the assignments in the spectra of Ga_9In_4. Because many of the

Fig. 11 The ^{1}H-NMR of 2 mM Ga_8In_5 in d_6-DMSO 1 day after dissolution with peak assignment. $H_{InInIn}^{\mu_3}$(A), $H_{InInGa}^{\mu_3}$(B), $H_{InGaIn}^{\mu_3}$(D), $H_{InInIn}^{\mu_2int}$(G), $H_{InInGa}^{\mu_2int}$(H), $H_{InGaIn}^{\mu_2int}$(J), $H_{InIn}^{\mu_2ext}$(M), $H_{InGa}^{\mu_2ext}$(N), $H_{GaIn}^{\mu_2ext}$(O).

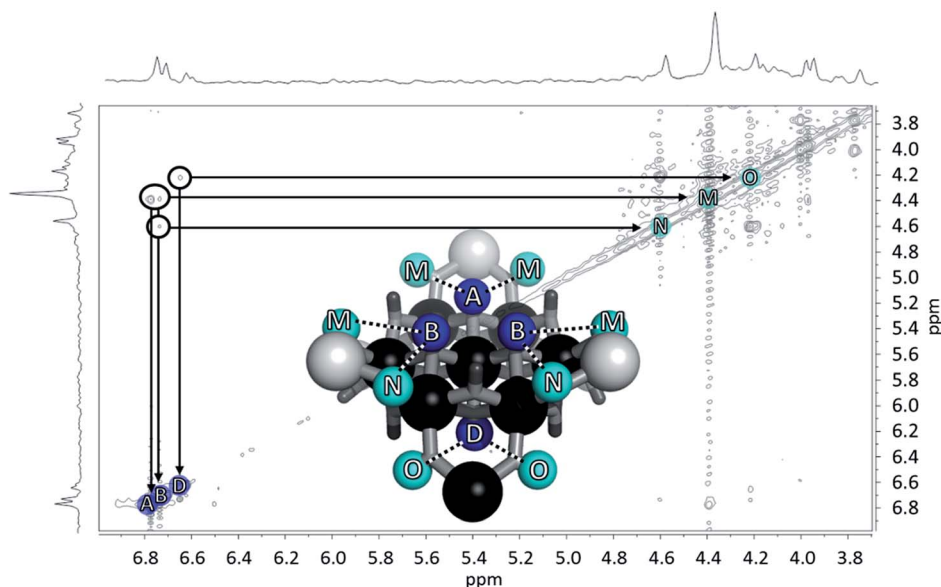**Fig. 12** The NOESY of Ga_8In_5 indicating the proper peak assignment of the $H_{InIn}^{\mu_2ext}$(M), $H_{InGa}^{\mu_2ext}$(N), and $H_{GaIn}^{\mu_2ext}$(O) protons. Water ligands have been omitted from the structure for clarity. ● Gallium, ○ indium, $H_{InInIn}^{\mu_3}$(A), $H_{InInGa}^{\mu_3}$(B), $H_{InGaIn}^{\mu_3}$(D).

peaks overlap with others, the integrations are no longer solely reliable for making full assignments. Therefore, the relative values of the computed NMR shifts were used alongside the known assignments from Ga_7In_6 and Ga_8In_5 for the most precise results. This allowed for the $H_{InIn}^{\mu_{2ext}}$ and $H_{GaGa}^{\mu_{2ext}}$ peaks to be distinguished, as well as the $H_{GaIn}^{\mu_{2int}}$ and $H_{GaInGa}^{\mu_{2int}}$ peaks (Fig. 14). For the $H_{InIn}^{\mu_{2ext}}$ and $H_{GaGa}^{\mu_{2ext}}$ peaks, computations showed that the $H_{InIn}^{\mu_{2ext}}$ peak should have a slightly downfield chemical shift compared to $H_{GaGa}^{\mu_{2ext}}$. Likewise, the computed shift for the $H_{GaInGa}^{\mu_{2int}}$ was compared to the signals from the other internal and external μ_2-OH protons. This analysis showed that I should have the farthest downfield shift of the internal μ_2-OH protons, but should not be higher than any of the external μ_2-OH protons. After determining the identity of the peaks in the Ga_9In_4 spectrum, this method was used to further assign the peaks in the spectra of the clusters with increasing gallium content.

While these computations were successful in reproducing the relative ordering of proton signals, the present method is not sufficient to quantitatively reproduce the exact proton shifts. This is because this method does not rely on quantum mechanically determined positions of the counterions with respect to the clusters. Quantitative predictions will necessitate a more rigorous method for determining the cluster–counterion complex. We suspect that the success of our method in being able to reproduce qualitative ordering of the proton peaks suggests that the counterions are loosely coordinated around the cluster and is dynamically equilibrating among the different sites in the NMR time scale. Work is continuing in this area to produce quantitative predictions from *ab initio* molecular dynamics simulations with explicit counterions and solvents.
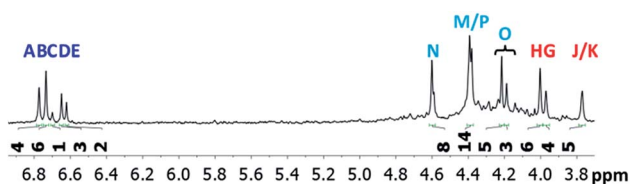
4.3 $Ga_{10}In_3$–Ga_{13}. Experimental data suggests that $Ga_{10}In_3$ also exists as three isomers but, in a 3 : 6 : 1 ratio leading to the peak integrations listed in Table 8. Unfortunately, the complexity caused by the increasing number of exterior gallium atoms and the isomers does not allow these signals to be assigned experimentally. Similar issues arise for $Ga_{11}In_2$ to Ga_{13}. Given the complexity of the signals arising from the protons in these clusters, computations are particularly useful for peak assignment.

Computed shifts were used to assign the remaining types of protons for each of these clusters (Fig. 15). Unfortunately, we are unable to compute the changes based on coordinated DMSO breaking the symmetry; therefore, only the peaks of the "mother cluster" (fully H_2O ligated) can be assigned in these spectra. Primarily, this involved computing the position of $H_{GaGaGa}^{\mu_{2int}}$, which represents the protons in a section of the cluster with three external gallium ions next to each other. Computed results suggest that $H_{GaGaGa}^{\mu_{2int}}$ should have the lowest shift of all of the internal μ_2-OH protons, which is the lowest ppm value for all of the computed signals.

Fig. 13 The ^{1}H-NMR of 2 mM Ga_9In_4 in d_6-DMSO 1 day after dissolution with experimental peak assignment. $H_{InInIn}^{\mu_3}$(A), $H_{InInGa}^{\mu_3}$(B), $H_{GaInGa}^{\mu_3}$(C), $H_{InGaIn}^{\mu_3}$(D), $H_{GaGaIn}^{\mu_3}$(E), $H_{InInIn}^{\mu_{2int}}$(G), $H_{InInGa}^{\mu_{2int}}$(H), $H_{InGaIn}^{\mu_{2int}}$(J), $H_{GaGaIn}^{\mu_{2int}}$(K), $H_{InIn}^{\mu_{2ext}}$(M), $H_{InGa}^{\mu_{2ext}}$(N), $H_{GaIn}^{\mu_{2ext}}$(O), $H_{GaGa}^{\mu_{2ext}}$(P).

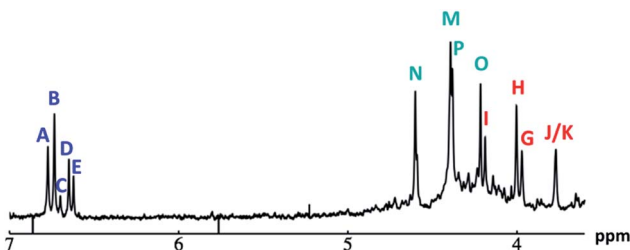**Fig. 14** The ^{1}H-NMR of 2 mM Ga_9In_4 in d_6-DMSO 1 day after dissolution with computed peak assignment. $H_{InInIn}^{\mu_3}$(A), $H_{InInGa}^{\mu_3}$(B), $H_{GaInGa}^{\mu_3}$(C), $H_{InGaIn}^{\mu_3}$(D), $H_{GaGaIn}^{\mu_3}$(E), $H_{InInIn}^{\mu_{2int}}$(G), $H_{InInGa}^{\mu_{2int}}$(H), $H_{GaInGa}^{\mu_{2int}}$(I), $H_{InGaIn}^{\mu_{2int}}$(J), $H_{GaGaIn}^{\mu_{2int}}$(K), $H_{InIn}^{\mu_{2ext}}$(M), $H_{InGa}^{\mu_{2ext}}$(N), $H_{GaIn}^{\mu_{2ext}}$(O), $H_{GaGa}^{\mu_{2ext}}$(P).

Fig. 15 Computed peak assignments for μ_3-OH and μ_2-OH proton signals are shown overlaid with ^{1}H-NMR spectra of 2 mM $Ga_{10}In_3$, $Ga_{11}In_2$, $Ga_{12}In_1$, and Ga_{13} cluster in d_6-DMSO one day after dissolution $H_{InInIn}^{\mu_3}$(A), $H_{InInGa}^{\mu_3}$(B), $H_{GaInGa}^{\mu_3}$(C), $H_{InGaIn}^{\mu_3}$(D), $H_{GaGaIn}^{\mu_3}$(E), $H_{GaGaGa}^{\mu_3}$(F), $H_{InInIn}^{\mu_{2int}}$(G), $H_{InInGa}^{\mu_{2int}}$(H), $H_{GaInGa}^{\mu_{2int}}$(I), $H_{InGaIn}^{\mu_{2int}}$(J), $H_{GaGaIn}^{\mu_{2int}}$(K), $H_{GaGaGa}^{\mu_{2int}}$(L), $H_{InIn}^{\mu_{2ext}}$(M), $H_{InGa}^{\mu_{2ext}}$(N), $H_{GaIn}^{\mu_{2ext}}$(O), $H_{GaGa}^{\mu_{2ext}}$(P).

Fig. 16 Stacked titration data indicating that only the $H_{GaGaGa}^{\mu_3}$(F), $H_{GaGaGa}^{\mu_{2int}}$(L), and $H_{GaGa}^{\mu_{2ext}}$ (P) protons translate from the 100% d_6-DMSO to th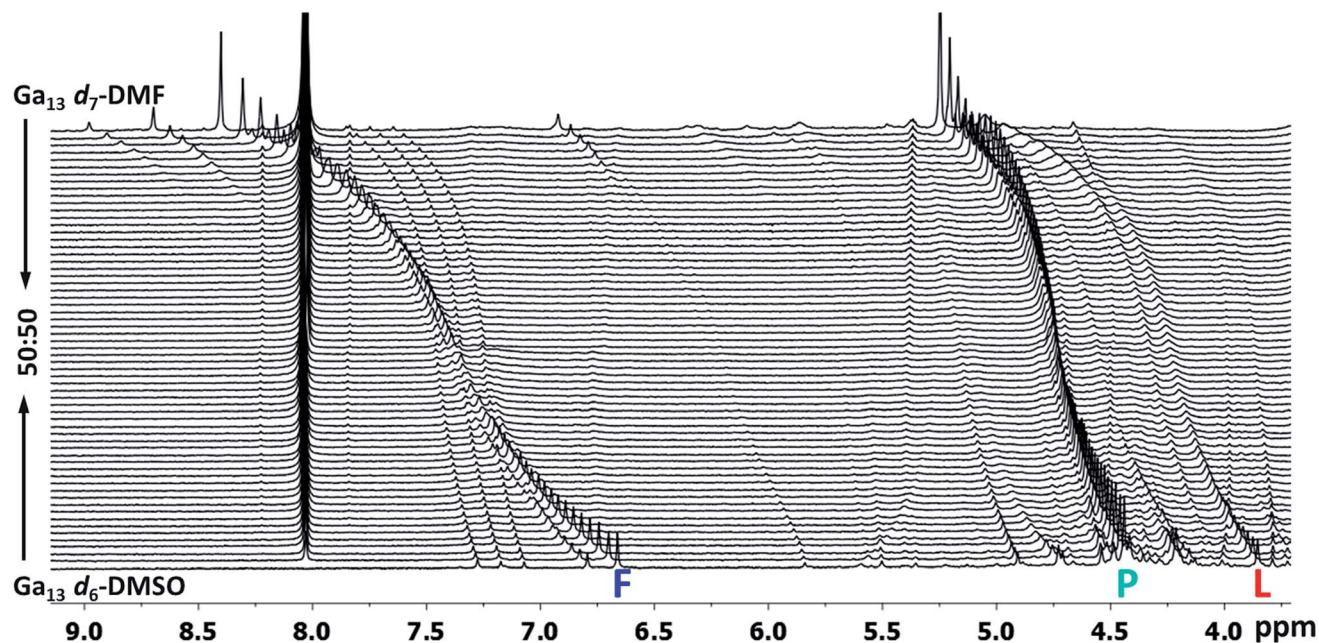e 100% d_7-DMF spectrum. The triplet that persists in the 7.0 to 7.5 ppm region is attributed to ammonia in the sample.[77]

The **Ga₁₃** mother cluster peaks ($H_{GaGaGa}^{\mu_3}$, $H_{GaGaGa}^{\mu_{2int}}$, and $H_{GaGa}^{\mu_{2ext}}$) assigned via computations were thereafter confirmed experimentally. By plotting the ^{1}H-NMR spectra of **Ga₁₃** dissolved in a variety of ratios of d_6-DMSO and d_7-DMF, it is clearly visible that only 3 peaks persist from 100% d_6-DMSO to 100% d_7-DMF (Fig. 16). The other peaks visible in the spectra are caused by "daughter clusters" substituted with either DMSO or DMF ligands at the aquo sites; therefore, the only shared species must be the mother cluster.

Conclusion

This research has led to quick and cost effective differentiation and structural characterization of the **Ga₁₃₋ₓInₓ** clusters in solution *via* ^{1}H-NMR spectrscopy.[77] We have shown that each mixed **Ga₁₃₋ₓInₓ** cluster does independently exist in solution and that there are no kinetically or enthalpically favored isomers (*i.e.*, only the expected statistical ratios of the various isomers were observed). These isomers exist in statistical ratios determined by probability of formation. In general, this study provides a complete method for experimentally and computationally predicting proton shifts for inorganic μ₃-OH and μ₂-OH signals in gallium and indium species, as well as, a literature review of hydroxide bridges for all diamagnetic metals available in the literature to the best of our knowledge. This knowledge will initiate the study of cluster dynamics in solution, allowing for better control and manipulation of precursor clusters. The solution behavior of clusters condensing into films is a primary interest of this research; however, inorganic cluster species are not only relevant to the thin film and electronics markets. Many small clusters, including the **Ga₁₃₋ₓIn₁₃** clusters have structures much like fragment of minerals. The reverse process, bulk

material breaking down into smaller components (*i.e.* minerals dissolving in acid rain) is a promising environment for locating dynamic clusters. It is possible that a plethora of clusters form naturally as minerals dissolve, but we have had no way of detecting these intermediate molecules. Geoscience may be greatly affected by the use of ^{1}H-NMR for the observation of inorganic –OH bridges. Al₁₃ Keggin and calcium carbonate clusters have both been detected in nature.[78,79] It would be beneficial for the geoscience community to investigate water samples from streams, caves, hot springs, geysers, and ocean vents for the presence of these observable hydroxo bridges. ^{1}H-NMR research on completely inorganic systems is limited, but this study shows that it can lead to a variety of information previously thought to be inaccessible.

Acknowledgements

Notes and references

1 R. J. Abraham, J. Fisher and P. Loftus, *Introduction to NMR Spectroscopy*, John Wiley & Sons Ltd, New York, 1988.

2 A. F. Oliveri, M. E. Carnes, M. M. Baseman, E. K. Richman, J. E. Hutchison and D. W. Johnson, *Angew. Chem., Int. Ed.*, 2012, **51**, 10992–10996.

3 J. W. Akitt, J. E. Elders, X. L. R. Fontaine and A. K. J. Kundu, *J. Chem. Soc., Dalton Trans.*, 1989, 1889–1895.

4 B. Y. A. Fratiello, R. E. Lee and R. E. Schuster, *Inorg. Chem.*, 1969, 82–85.

5 M. C. Read, J. Glaser, M. Sandstrom and I. Toth, *Inorg. Chem.*, 1992, **31**, 4155–4159.

6 A. Fratiello, S. Peak, R. Schuster and D. J. Davis, *J. Phys. Chem.*, 1970, **74**, 3730–3734.

7 J. W. Akitt and J. M. J. Elders, *J. Chem. Soc., Dalton Trans.*, 1988, 1347–1355.

8 J. R. Houston, B. L. Phillips and W. H. Casey, *Geochim. Cosmochim. Acta*, 2006, **70**, 1636–1643.

9 G. S. Papaefstathiou, A. Sofetis, C. P. Raptopoulou, A. Terzis, G. Spyroulias and T. F. J. Zafiropoulos, *J. Mol. Struct.*, 2007, **837**, 5–14.

10 P. Hodge and B. Piggott, *Chem. Commun.*, 1998, **4**, 1933–1934.

11 S. Ogo, N. Makihara and Y. Watanabe, *Organometallics*, 1999, **18**, 5470–5474.

12 K. M. Carlson-Day, J. L. Eglin, L. T. Smith and R. J. Staples, *Inorg. Chem.*, 1999, **38**, 2216–2220.

13 Z. L. Mensinger, J. T. Gatlin, S. T. Meyers, L. N. Zakharov, D. A. Keszler and D. W. Johnson, *Angew. Chem., Int. Ed.*, 2008, **47**, 9484–9486.

14 Z. L. Mensinger, W. Wang, D. A. Keszler and D. W. Johnson, *Chem. Soc. Rev.*, 2012, **41**, 1019–1030.

15 M. K. Kamunde-Devonish, M. N. Jackson, Z. L. Mensinger, L. N. Zakharov and D. W. Johnson, *Inorg. Chem.*, 2014, **53**, 7101–7105.

16 M. N. Jackson, L. A. Wills, I.-Y. Chang, M. E. Carnes, L. F. Scatena, P. H.-Y. Cheong and D. W. Johnson, *Inorg. Chem.*, 2013, **52**, 6187–6192.

17 W. G. Jackson, J. A. McKeon, M. Zehnder, M. Neuberger and S. Fallab, *Chem. Commun.*, 2004, **6**, 2322–2323.

18 D. Schweinfurth, J. Klein, S. Hohloch, S. Dechert, S. Demeshko, F. Meyer and B. Sarkar, *Dalton Trans.*, 2013, **42**, 6944–6952.

19 I. Bernal, J. Cetrullo and S. J. Berhane, *Coord. Chem.*, 2000, **52**, 185–205.

20 N. Juranic and S. Macura, *Inorg. Chim. Acta*, 2000, **298**, 103–106.

21 P. Angus, D. Fairlie, R. Gunasingam, Z. Tao and W. G. Jackson, *Inorg. Chim. Acta*, 1993, **209**, 123–127.

22 J. W. Akitt and R. H. J. Duncan, *J. Chem. Soc., Faraday Trans. 1*, 1980, **76**, 2212.

23 J. a. Tossell, *J. Magn. Reson.*, 1998, **135**, 203–207.

24 J. P. Canal, M. Jennings, G. P. A. Yap and R. K. Pomeroy, *Dalton Trans.*, 2008, 1375–1382.

25 S. M. T. Abedin, K. A. Azam, M. B. Hursthouse, S. E. Kabir, K. M. A. Malik, R. Miah and H. J. Vahrenkamp, *Organomet. Chem.*, 1998, **564**, 133–141.

26 J. Ruiz, C. Vicente, J. Marti, N. Cutillas, G. Garcia and G. J. Lopez, *Organomet. Chem.*, 1993, **460**, 241–248.

27 G. Lopez, J. Ruiz, G. Garcia, C. Vicente, J. Casab, E. Molins and C. Miravitlles, *Inorg. Chem.*, 1991, **30**, 2605–2610.

28 G. Sanchez, J. Serrano, J. Garcia, G. Lopez, J. Perez and E. Molins, *Inorg. Chim. Acta*, 1999, **287**, 37–46.

29 V. M. Nosova, Y. A. Ustynyuk, L. G. Bruk, O. N. Temkin, A. V. Kisin and P. A. Storozhenko, *Inorg. Chem.*, 2011, **50**, 9300–9310.

30 J. L. Serrano, I. J. S. Fairlamb, G. Sánchez, L. García, J. Pérez, J. Vives, G. López, C. M. Crawforth and R. J. K. Taylor, *Eur. J. Inorg. Chem.*, 2004, 2706–2715.

31 A. Bandini, G. Banditelli, M. A. Cinellu, G. Sanna, G. Minghetti, F. Demartin and M. Manassero, *Inorg. Chem.*, 1989, **28**, 404–410.

32 P. Bergamini, S. Sostero, O. Traverso, T. J. Kemp and P. G. J. Pringle, *J. Chem. Soc., Dalton Trans.*, 1989, 2017–2021.

33 B. Longato, D. Montagner, G. Bandoli and E. Zangrando, *Inorg. Chem.*, 2006, **45**, 1805–1814.

34 A. Bandini, G. Banditelli, F. Demartin, M. Manassero and G. Minghetti, *Gazz. Chim. Ital.*, 1993, **123**, 417–423.

35 J. Schneider, J. Hagen, N. Czap, C. Kruger, S. Mason, R. Bau, J. Ensling, P. Gutlich and B. Wrackmeyer, *Chem.–Eur. J.*, 2000, **6**, 625–635.

36 L. Dostál, J. Taraba and R. J. Jambor, *Organomet. Chem.*, 2009, **694**, 1251–1253.

37 R. Zhang, Q. Zhang, Y. Shi and C. J. Ma, *Organomet. Chem.*, 2006, **691**, 1668–1672.

38 C. Ma, J. Li, R. Zhang and L. J. Qiu, *J. Mol. Struct.*, 2007, **830**, 1–7.

39 C. Eychenne-Baron, F. Ribot, S. Nathalie and C. Sanchez, *Organometallics*, 2000, **19**, 1940–1949.

40 S. Mishra, S. Daniele, L. G. Hubert-Pfalzgraf and E. Jeanneau, *Eur. J. Inorg. Chem.*, 2007, **15**, 2208–2215.

41 E. Asato, H. Furutachi, T. Kawahashib and M. J. Mikuriyab, *J. Chem. Soc., Dalton Trans.*, 1995, 3897–3904.

42 D. L. Reger, A. E. Pascui, P. J. Pellechia and M. D. Smith, *Inorg. Chem.*, 2013, **52**, 11638–11649.

43 A. Tarushi, F. Kastanias, V. Psycharis, C. P. Raptopoulou, G. Psomas and D. P. Kessissoglou, *Inorg. Chem.*, 2012, **51**, 7460–7462.

44 W. Teng, M. Guino-o, J. Hitzbleck, U. Englich and K. Ruhlandt-Senge, *Inorg. Chem.*, 2006, **45**, 9531–9539.

45 F. A. Cotton, L. M. Daniels, G. T. Jordan, C. Lin and C. A. Murillo, *Inorg. Chem. Commun.*, 1998, **1**, 109–110.

46 P. Rosendorfer and W. Beck, *Chem. Ber.*, 1995, **128**, 729–734.

47 J. Cook, J. Hamilin, A. Nutton and P. M. J. Maitlis, *J. Chem. Soc., Dalton Trans.*, 1981, 2342–2352.

48 D. Walther, B. Ritter, H. Gorls and G. Z. Zahn, *Z. Anorg. Allg. Chem.*, 1997, **623**, 1125–1130.

49 R. Zhang, C. Li, Q. Wang and M. Chunlin, *Struct. Chem.*, 2010, **21**, 745–753.

50 R. J. Wehmschulte, J. M. Steele and M. A. Khan, *Organometallics*, 2003, **22**, 4678–4684.

51 M. Stender and P. P. Power, *Polyhedron*, 2002, **21**, 525–529.

52 D. F. Jones, P. H. Dixneuf, A. Benoit and J. Le Marouille, *Inorg. Chem.*, 1983, **22**, 29–33.

53 Y. J. Park, S. A. Cook, N. S. Sickerman, Y. Sano, J. W. Ziller and A. S. Borovik, *Chem. Sci.*, 2013, **4**, 717–726.

54 A. Preetz, W. Baumann, H.-J. Drexler, C. Fischer, J. Sun, A. Spannenberg, O. Zimmer, W. Hell and D. Heller, *Chem.–Asian J.*, 2008, **3**, 1979–1982.

55 L. Wang, T. Sheng, J. Zhang, S. Hu, R. Fu, X. Wu, Y. Li, X. Huang and S. Xiang, *Polyhedron*, 2007, **26**, 1098–1104.

56 M. Vasiliu, K. E. Knope, L. Soderholm and D. A. J. Dixon, *J. Phys. Chem. A*, 2012, **116**, 6917–6926.

57 S. Mishra, E. Jeanneau, S. Daniele and L. G. Hubert-Pfalzgraf, *CrystEngComm*, 2008, **10**, 814–816.

58 S. Mishra, L. G. Hubert-Pfalzgraf, S. Daniele, M. Rolland, E. Jeanneau and B. Jouguet, *Inorg. Chem. Commun.*, 2009, **12**, 97–100.

59 J. Martinez, I. Aiello, A. Bellusci, A. Crispini and M. Ghedini, *Inorg. Chim. Acta*, 2008, **361**, 2677–2682.

60 P. G. Parzuchowski, J. W. Kampf, E. Roźniecka, Y. Kondratenko, E. Malinowska and M. E. Meyerhoff, *Inorg. Chim. Acta*, 2003, **355**, 302–313.

61 H. Hoveyda, S. Rettig and C. Orvig, *Inorg. Chem.*, 1993, **32**, 4909–4913.

62 W. Wang, K. M. Wentz, S. E. Hayes, D. W. Johnson and D. A. Keszler, *Inorg. Chem.*, 2011, **50**, 4683–4685.

63 M. J. Frisch, G. W. Trucks, H. B. Schlegel, G. E. Scuseria, M. A. Robb, J. R. Cheeseman, J. A. Montgomery Jr, T. Vreven, K. N. Kudin, J. C. Burant, J. M. Millam, S. S. Iyengar, J. Tomasi, V. Barone, B. Mennucci, M. Cossi, G. Scalmani, N. Rega, G. A. Petersson, H. Nakatsuji, M. Hada, M. Ehara, K. Toyota, R. Fukuda, J. Hasegawa, M. Ishida, T. Nakajima, Y. Honda, O. Kitao, H. Nakai, M. Klene, X. Li, J. E. Knox, H. P. Hratchian, J. B. Cross, V. Bakken, C. Adamo, J. Jaramillo, R. Gomperts, R. E. Stratmann, O. Yazyev, A. J. Austin, R. Cammi, C. Pomelli, J. W. Ochterski, P. Y. Ayala, K. Morokuma, G. A. Voth, P. Salvador, J. J. Dannenberg, V. G. Zakrzewski, S. Dapprich, A. D. Daniels, M. C. Strain, O. Farkas, D. K. Malick, A. D. Rabuck, K. Raghavachari, J. B. Foresman, J. V. Ortiz, Q. Cui, A. G. Baboul, S. Clifford, J. Cioslowski, B. B. Stefanov, G. Liu, A. Liashenko, P. Piskorz, I. Komaromi, R. L. Martin, D. J. Fox, T. Keith, M. A. Al-Laham, C. Y. Peng, A. Nanayakkara, M. Challacombe, P. M. W. Gill, B. Johnson, W. Chen, M. W. Wong, C. Gonzalez, and J. A. Pople. *Gaussian*, 2004.

64 Data is shown for clusters in solution one day after dissolution because this is the relative amount of time it takes for the outer ligand shell to equilibrate with incoming DMSO ligands of solvation at room temperature.

65 A. F. Oliveri, E. W. Elliott, M. E. Carnes, J. E. Hutchison and D. W. Johnson, *ChemPhysChem*, 2013, **14**, 2655–2661.

66 *The Group 13 Metals Aluminium, Gallium, Indium, and Thallium: Chemical Patterns and Peculiarities*, ed. AldridgeS. and DownsA. J., A John Wiley and Sons, Ltd., Chichester, 2011, pp. 52–55.

67 P. C. Hariharan and J. A. Pople, *Theor. Chim. Acta*, 1973, **28**, 213–222.

68 W. J. Hehre, R. Ditchfield and J. A. Pople, *J. Chem. Phys.*, 1972, **56**, 2257–2261.

69 P. J. Hay and W. R. Wadt, *J. Chem. Phys.*, 1985, **82**, 299–310.

70 P. J. Hay and W. R. Wadt, *J. Chem. Phys.*, 1985, **82**, 270–283.

71 F. Weigend and R. Ahlrichs, *Phys. Chem. Chem. Phys.*, 2005, **7**, 3297–3305.

72 A. Klamt and G. Schüürmann, *J. Chem. Soc., Perkin Trans. 1*, 1993, **2**, 799–805.

73 B. Mennucci and J. Tomasi, *J. Chem. Phys.*, 1997, **106**, 5151–5158.

74 A. Klamt and G. Schüürmann, *J. Chem. Soc., Perkin Trans. 2*, 1993, 799–805.

75 Due to a small impurity in **Ga₁₁In₂**, the spectra could not accurately be integrated; therefore, the experimental percentages were not calculated.

76 T. D. W. Claridge, *High-Resolution NMR Techniques in Organic Chemistry*, Elsevier, Oxford, 2nd edn, 2009, pp. 303–334.

77 M. E. Carnes, C. C. Knutson, A. Nadarajah, M. N. Jackson, A. F. Oliveri, K. M. Norelli, B. M. Crockett, S. R. Bauers, H. A. Moreno-Luna, B. N. Taber, D. J. Pacheco, J. Z. Olson, K. R. Brevick, C. E. Sheehan, D. W. Johnson and S. W. Boettcher, *J. Mater. Chem. C*, 2014, **2**, 8492–8496.

78 G. Furrer, B. L. Phillips, K.-U. Ulrich, R. Pöthig and W. H. Casey, *Science*, 2002, **297**, 2245–2247.

79 D. Gebauer, A. Völkel and H. Cölfen, *Science*, 2008, **322**, 1819–1822.